FOOTAGE FIRM, INC.

Radar Taking Off

Philipp Hügler, Fabian Roos, Markus Schartel, Martin Geiger, and Christian Waldschmidt

Modern consumer and industrial unmanned aerial vehicles (UAVs) are easy-to-use flying sensor platforms. They offer stable flight, good maneuverability, hovering, and even waypoint flights in autopilot mode. For stabilization and localization, sensors such as inertial measurement units (IMUs)—including gyroscopes and accelerometers—barometric sensors, and the Global Navigation Satellite System (GNSS) are used. To sense the UAV's direct environment, e.g., for collision avoidance or fully automated flight, additional sensors are needed. State-of-the-art combinations of infrared,

Philipp Hügler (Philipp.Hügler@uni-ulm.de), Fabian Roos (Fabian.Roos@uni-ulm.de), Markus Schartel (Markus.Schartel@uni-ulm.de), Martin Geiger (Martin.Geiger@uni-ulm.de), and Christian Waldschmidt (Christian.Waldschmidt@uni-ulm.de) are with the Institute for Microwave Technology, University of Ulm, Germany.

Digital Object Identifier 10.1109/MMM.2018.2862558

Date of publication: 12 October 2018

Radar sensors are particularly beneficial when it comes to environments in which metallic objects need to be inspected, such as power lines or structural steel in reinforced concrete.

ultrasonic, and vision-based sensors (monocular and/or stereo vision) capture the close vicinity. Using radar sensors is advantageous, as they are able to directly sense range and velocity and are not affected by lighting conditions and contrast. With the help of a multichannel radar, the angular information may also be extracted.

UAVs can lift a considerable payload with respect to their size. All of their characteristics, combined with radar sensors, make them a promising tool for a large variety of applications.

Application Areas

In industrial environments, UAVs equipped with a combination of visible-light and thermal cameras are used for inspection purposes in areas that are difficult to access, including power lines, structures (e.g., bridges), and wind turbines [1]. Cameras and light detection and ranging (lidar) sensors are used in forestry to estimate tree canopy heights [2], woody-tree abundance, or even species diversity [3]. Radar sensors are particularly beneficial when it comes to environments in which metallic objects need to be inspected, such as power lines or structural steel in reinforced concrete.

Figure 1. *A DHL Parcelcopter 2.0 approaching the German island of Juist in the North Sea. (Photo courtesy of Deutsche Post AG.)*

Figure 2. *An octacopter spraying a field.*

Parcel services are very interested in UAVs because of the possibility of fast and autonomous delivery, even in remote areas. For example, autonomous delivery flights by a Parcelcopter connecting the harbor of Norddeich, Germany, and the North Sea island of Juist are being tested by Deutsche Post DHL Group [4] to perform emergency delivery of medications (Figure 1). The 12-km route is used when no alternative transport, such as ferries or conventional planes, is available because of low water or heavy fog. Newer approaches use a copter-based last-mile delivery in alpine regions, with a parcel station handling the Parcelcopter's automated loading and offloading [5]. Increasing autonomy demands reliable safety features, with radar offering excellent performance in terms of distant obstacle detection and collision avoidance, particularly under conditions where other sensors fail.

According to [6], the agriculture industry is the biggest worldwide commercial market for UAVs. Unmanned aircraft can monitor field conditions and plant health with an easy-to-handle setup and capture images at a higher resolution than satellites, even under cloudy conditions. UAVs are also used to spray fertilizer or pesticide [7], as shown in Figure 2. For such applications, the distance between the UAV and the plants must be kept constant to assure uniform spraying. This can be achieved using a radar, as shown in [8]. In addition, radar—i.e., ground-penetrating radar (GPR)—is the only sensor concept able to perform subsurface measurements [9]; it could be used to prevent harvesters from being damaged by buried metal objects.

Barometric sensors and GNSS do not fulfill this requirement. Vision-based sensors for altitude evaluation and collision avoidance can be precisely operated at 0.1–8 m downward-looking and 0.5–12 m forward-looking, and they have a maximum detectable range of up to 30 m [10]. But they often have difficulties with regular surface patterns, and the performance depends on the reflectivity of the material and the illumination. With radar sensors, on the other hand, one can detect not only the altitude above ground level (AGL) but also obstacles such as vegetation [11]. Radar can directly measure the velocity of obstacles, has a large detectable maximum range, and is robust regarding weather influences. For these reasons, drone manufacturers now offer radar sensors at 24 GHz for terrain following as well as collision avoidance [7], [12].

UAVs and Radar: Remote Sensing and Safety Improvement

Because of UAVs' significant flexibility, they are quite interesting for remote-sensing applications. In the field of radar sensors, synthetic aperture radar (SAR) is used to enhance the aperture, resulting in high angular resolution. Larger UAVs, e.g., with a maximum weight of 85 kg, have already been equipped with a 94-GHz SAR with 1-GHz bandwidth [13]. The potential for sensing small-scale features, as shown in Figure 3, is leading to the use of SAR with smaller consumer drones (fewer than 5 kg). In [14]–[16], commercial, off-the-shelf pulse radar sensors with a frequency range of 3.1–5.3 GHz were used for surface and subsurface imaging.

A platform using a 24-GHz frequency-modulated continuous wave (FMCW) radar with a 250-MHz bandwidth for full interferometric SAR imaging and processing was evaluated in [17]. In [9], an approach was presented for UAV-based mine detection using ground-penetrating SAR. It was shown that a real-time kinematic (RTK) GNSS is required for the demanding position accuracy necessary when using a 1–4-GHz ultrawide-band FMCW radar to detect targets with low reflectivity. Besides remote sensing, radar can also be used to improve safety features for UAVs. Radar can detect obstacles for collision avoidance and surface monitoring, even in low-contrast situations and under severe surrounding conditions, e.g., with backlight.

An easy way to detect moving targets is to use a Doppler radar, as in [18], which operates in the X-band at a frequency of 10.5 GHz. In addition to the detection of moving targets, Doppler signatures are used to identify previously characterized aircraft. However, this setup is not suitable for evaluating the distance to the targets. With FMCW modulation, the distance as well as the velocity can be measured. The measurements in [19] showed the potential of a 24-GHz FMCW radar with 1-GHz bandwidth for potential intruder and ground target detection. But the device in this case was mounted not on a UAV but on a stationary or moving ground station.

Increasing autonomy demands reliable safety features, with radar offering excellent performance in terms of distant obstacle detection and collision avoidance.

Sensing of the altitude AGL with a 24-GHz FMCW radar and its fusion with accelerometer data were validated indoors using a motion-capture system consisting of 24 cameras [20]. An in-depth analysis of a 77-GHz radar-based altimeter was given in [11]. With 2-GHz bandwidth, 15 measurements/s, and an effective isotropic radiated power (EIRP) of approximately 1 W, a number of different experiments were performed. It was shown that a constant false alarm rate (CFAR) algorithm can reliably detect altitudes up to 40 m over grass. In addition, the influence of tilting caused by acceleration of the UAV was examined; an example for a roll angle of 17° is depicted in Figure 4. Despite the degradation of the signal-to-noise ratio by 10 dB, not only the ground but also the crop are visible. The same is valid for other vegetation, such as trees. Because of the high bandwidth, even single steps of stone masonry (between 20 and 25 cm high) can be resolved.

To reduce hardware complexity and thus achieve lower costs, a pulse-correlation radar can be used for altitude AGL estimation. In [8], a 26-GHz radar having

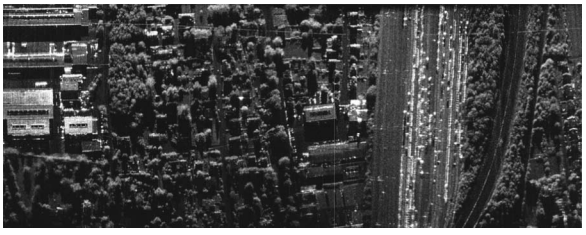

Figure 3. *A UAV SAR image of urban terrain taken with a MIRANDA radar, offering 1-GHz bandwidth. (Used with permission from [13].)*

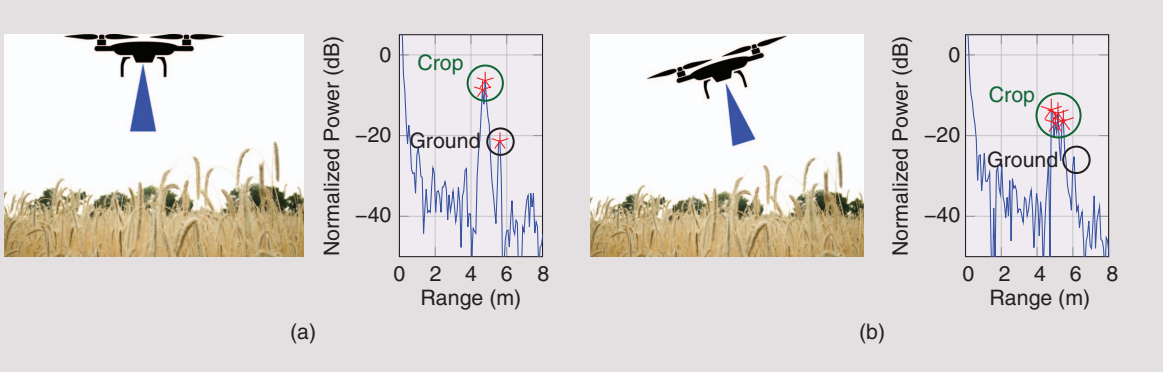

Figure 4. *The influence of the roll angle on altitude AGL measurements for a 77-GHz FMCW radar altimeter with an angle of (a) 0° and (b) 17°. Detected targets are marked with *.*

Radar can directly measure the velocity of obstacles, has a large detectable maximum range, and is robust regarding weather influences.

an update rate of up to 40 Hz, used in conjunction with a particle filter to track the altitude AGL, was compared with a low-cost lidar and an RTK GNSS. As Figure 5(b) shows, in the presence of vegetation between the UAV and the ground, the radar outperforms the lidar, which measures the distance to the vegetation instead of the altitude AGL.

To improve obstacle detection and collision avoidance, measuring radial velocity and the distance of targets is not enough. It would be useful to have at least the azimuth angular or direction-of-arrival (DoA) data to obtain two-dimensional spatial information concerning the location of the potential obstacle. The increasing use of radar in the automotive industry [21], [22] has led to a considerable decrease in cost and a high level of integration. Complete radar front ends in a single package, including antennas, are available in the industrial, scientific, and medical (ISM) bands at 60 and 122 GHz for industrial applications [23]–[25], making the realization of small form factor and lightweight radar sensors feasible for UAV applications.

Seeing Even More with Imaging Radar

For collision avoidance, an imaging radar has to fulfill several requirements. The separability of targets in the range direction is important, so a resolution in the single-digit-centimeter range is desirable. Assuming a maximum velocity v_{drone} of the UAV of ± 15 m/s, an unambiguous velocity of at least v_{drone} for stationary and $2v_{\text{drone}}$ for moving targets should be achieved. For classification purposes, a high Doppler resolution would be advantageous. To gain high angular resolution, an adequate number of channels is required.

Extracting Range and Velocity: The Modulation Format Used

Because of the expected multitarget scenario, the notion of an FMCW radar with fast ramps (also called *chirp-sequence frequency modulation* [26]) is chosen as the operating principle of the imaging radar. As the radar transmits several sawtooth-shaped ramps (called a *block*), range and velocity can be extracted using a two-dimensional Fourier transform (FT) [27]. Because of the fast ramps, the velocity influence can be neglected for the range calculation, realized by a first FT over each ramp. With a second FT over several ramps, the motion-induced phase change from ramp to ramp can be extracted; this is proportional to the velocity.

At a carrier frequency f_c of 76.5 GHz, a bandwidth B of 2 GHz is chosen to achieve a range resolution Δr of 75 mm. The maximum unambiguous velocity v_{max} is limited by the ramp repetition interval T_{RRI} and is set to 60 μs, resulting in ± 16 m/s $= v_{\text{max}}$, which is higher than v_{drone}. The chirp duration T_c is 50 μs, which is evaluated for range extraction. The overall measurement time (the time of a single block) determines the velocity resolution Δv and results from the number of chirps L per block multiplied by T_{RRI}. A summary of the modulation parameters used and the resulting radar performance appears in Table 1.

In the following experiments, only stationary or slow-moving targets are considered, so the used T_{RRI} is sufficient. For applications with higher relative velocity, decreasing T_{RRI} and B by a factor of two would double v_{max} and halve Δr. This would not change the maximum expected intermediate frequency; therefore, the sampling frequency could remain the same.

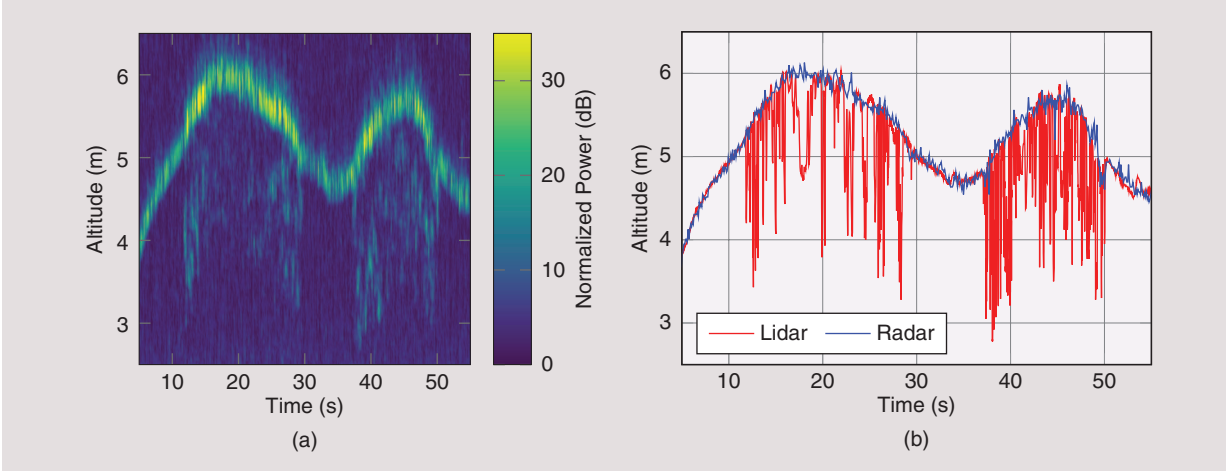

Figure 5. *A comparison of the altitude AGL measurements of a 26-GHz pulse-correlation radar with particle filter and lidar when flying over a cornfield: (a) the radar data from a flight above a cornfield and (b) the altitude AGL from radar data with a particle filter versus lidar data [8].*

The Way to Imaging Radar: DoA Estimation

For high angular resolution, a large aperture is needed. Because of the limited space and weight when attached to a UAV, a multiple-input, multiple-output (MIMO) radar can be used to generate a large virtual aperture with a limited number of transmitters and receivers. Several orthogonal waveforms for FMCW radars are discussed in [28]. Here, time-division multiplexing (TDM) was applied, achieving orthogonality by switching transmitters consecutively on and off, with only one transmitter active at a time. For the actual DoA estimation, there are several techniques available, as discussed in [29]–[31].

The radar has four transmitters and eight receivers on one printed circuit board (PCB). The antenna system is placed on an extra PCB to allow different antenna setups without the need to remanufacture the radar board. The transition between both PCBs is realized by a PCB-to-waveguide transition using a coplanar patch radiating in the H-plane of a WR10 waveguide (compare to [32]). The transition is available in two versions: one for down-facing antenna arrays and one for forward-facing arrays.

Figure 6(a) depicts the antenna front end employed in the following experiments. It uses three transmitters and eight receivers. The positions of the elements are chosen in such a way that, by the convolution of the transmitter positions with the receiver positions, a 24-element uniform linear array (ULA) is obtained as a virtual aperture [Figure 6(b)] [33]. The ULA has a ±90° ambiguity-free region, low sidelobe levels, and straightforward DoA estimation. The single channels are realized with series-fed patch antennas having 12-dBi gain and a 3-dB beamwidth of ±40° in azimuth and ±7° in elevation, which is considered the minimum field of view (FoV).

TDM MIMO Limitations and Their Compensation

Compared to other orthogonal waveforms, TDM MIMO comes with low hardware efforts but introduces a phase error when a movement by the targets and/or the radar is present during switching between transmitters. This phase error leads to inaccurate or even completely unusable angular estimation. One way to overcome this problem is to realize a virtual aperture with overlapping elements where the phase offset between the different active transmitters can be directly measured [34]. As Figure 6(b) shows, no overlapping element is used here to maximize the virtual aperture. The phase error in this case is fully compensated for with no extra effect by adapting the FT processing, as presented in [35].

Radar—i.e., ground-penetrating radar—is the only sensor concept able to perform subsurface measurements.

For UAV-based collision avoidance, the TDM scheme reduces the maximum unambiguous velocity

$$v_{\max} = \pm \frac{c}{2f_c} \frac{1}{2MT_{\mathrm{RRI}}} \tag{1}$$

by the number of used transmitters M. With the solution presented in [36], the same unambiguous Doppler

TABLE 1. A summary of the modulation parameters used and the resulting radar performance in range and velocity.

Parameter	Value
Carrier frequency f_c	76.5 GHz
Bandwidth B	2 GHz
Chirp duration T_c	50 μs
Ramp repetition time T_{RRI}	60 μs
Number of chirps L	258
Radar Performance	
Range resolution Δr	75 mm
Maximum unambiguous velocity $v_{\max}$	±16 m/s
Velocity resolution Δv	±13 cm/s

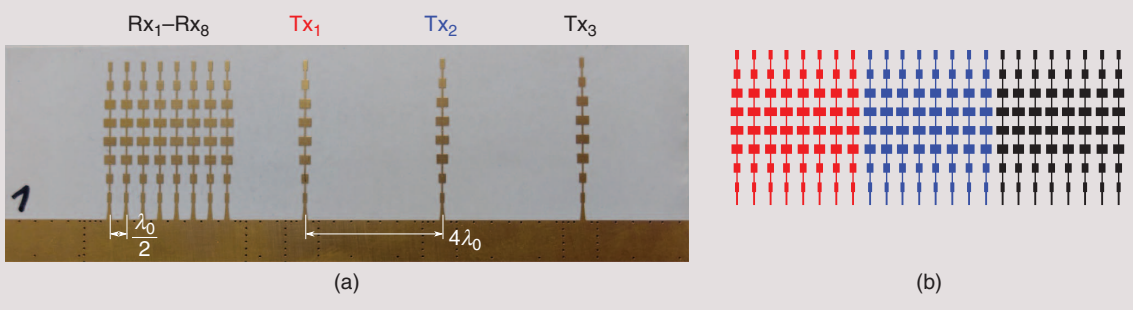

Figure 6. *(a) A fabricated antenna array on a PCB and (b) the resulting virtual aperture of the antenna array with three transmitters (Tx) and eight receivers (Rx). λ_0 is the free-space wavelength.*

High flexibility and easy usability boost the popularity of UAVs in consumer and industrial applications, ranging from autonomous parcel delivery to agriculture.

velocity as for the single-input, multiple-output case can be achieved with phase evaluation of the virtual aperture. Applying these compensation techniques to the signal processing chain of the TDM MIMO radar fulfills all previously specified requirements for UAV-based collision avoidance and environment sensing.

Measurement System and Target Extraction

The UAV used for the measurements is a DJI Matrice 600 Pro hexacopter. It offers high reliability, with three redundant IMUs and GNSS systems, and can lift a payload of up to 6 kg, with a flight time of approximately 15 min. If higher positional accuracy is needed, an RTK GNSS can be mounted. The telemetry data provided by the drone are captured at 50 Hz. The imaging radar and a custom-made measurement personal computer (PC) are mounted to the drone. The raw time-domain data are simultaneously sampled with an eight-channel analog-to-digital converter (ADC) card connected to a peripheral component interconnect express (PCIe) 3.0×8 slot. The sampling clock is coherently derived from the radar reference clock. For each transmitted set of frequency chirps, an industrial camera mounted to the UAV is hardware-triggered to obtain a picture of the measured scenario. The PC is built around a micro-ITX mainboard and features a low thermal design power Core i7 central processing unit with 16 GB of random-access memory and a solid-state drive (connected to a PCIe 3.0×4) for fast data rates of up to 1.5 GB/s. The PC with the imaging radar mounted on top is depicted in Figure 7.

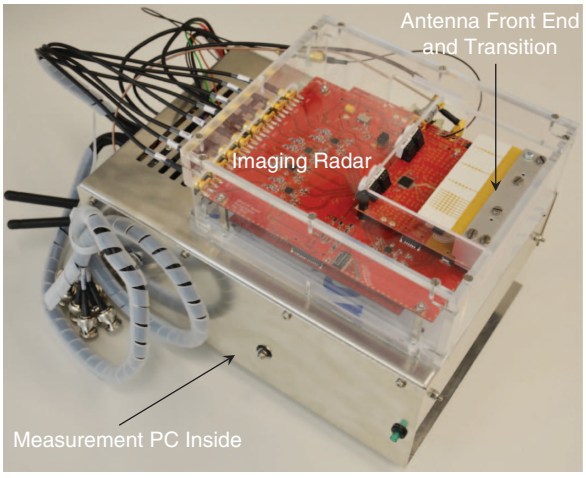

Figure 7. *The imaging radar mounted on the measurement PC.*

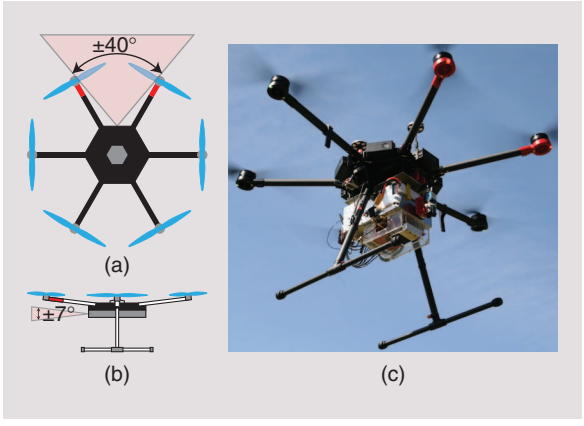

Figure 8. *The minimum FoV of the imaging radar: (a) a top view (azimuth) and (b) a side view (elevation). (c) The complete UAV with the mounted imaging radar sensor and the measurement PC.*

Live status information on the sampling card, telemetry script, and overall measurement status as well as the actual camera image are transmitted over the video link of the Matrice 600 Pro to a smartphone connected to the UAV remote controller. The complete system and additional sketches of the UAV showing the area covered by the antennas' FoV are depicted in Figure 8.

After analog-to-digital conversion of the raw data, the time-domain data are zero-padded by a factor of two, and the data of a complete block, consisting of 258 frequency chirps, are arranged in a three-dimensional (3-D) array. A Hann window is applied to all three dimensions. A linear prediction algorithm is used, and the DoA estimation is applied to each range-Doppler cell for better visualization, using a Bartlett beamformer. With a 3-D FT, the range, velocity, and angular data can be calculated. A CFAR algorithm is applied to the range–velocity data to extract possible targets. The radar measurement, video image, and telemetry data are synchronized by a GNSS time stamp. The radar specifications are summarized in Table 2.

The following section presents two scenarios with the imaging radar facing down. Subsequently, we investigate two different scenarios for obstacle avoidance with the imaging radar facing forward.

Downward-Facing Measurements

In the case of downward-facing measurements, the antenna beam in azimuth covers the x axis, and the antenna beam in elevation covers the y axis (compare to Figure 9). This setup can be used to obtain terrain profiles, sense any vegetation present, find suitable sites for planned or emergency landings, and keep a constant altitude AGL.

The first scenario presents a UAV takeoff on a meadow. The ground profile (xz plane) is shown in Figure 10(a). With the measured roll angle of approximately 0.5° based on IMU data, we can see that the UAV takeoff area is located on a slightly descending surface. Additional targets at a distance of up to 1 m are also visible. These arise from direct transmitter–receiver leakage and from the landing skid, which is not yet retracted [compare to Figure 10(c)].

From the range–velocity plot in Figure 10(b), the takeoff movement is clearly observable. Several targets with velocities around 0.5 m/s are visible in the range from –1.8 to –3 m. In contrast to the DoA estimation, only the radial distance and velocity can be evaluated, so this distribution of targets is expected. Targets that are farther away also have a lower velocity. This is caused by the Doppler dependency on the cosine of the incidence angle. In addition, the landing skid being retracted is visible in the range–velocity

TABLE 2. A summary of the radar parameters, including information about the MIMO scheme used, available number of transmitters and receivers, and information on the antenna.

Parameter	Value
Modulation	Chirp sequence
Sampling frequency	20 MHz
ADC resolution	14 bit
Update rate	15 Hz
MIMO scheme	TDM
Number of transmitters	Three used, four available
Number of receivers	Eight
EIRP	17 dBm
Virtual aperture	24-element ULA
Antenna gain	12 dBi
Minimum FoV azimuth	±40°
Minimum FoV elevation	±7°

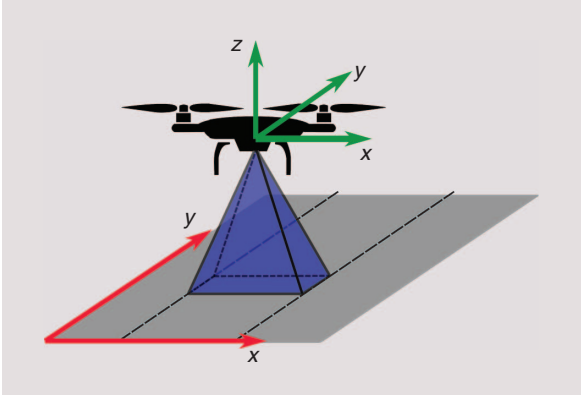

Figure 9. *The coordinate system used for all the measurements, with the illuminated area sketched in the case of a downward-facing antenna array.*

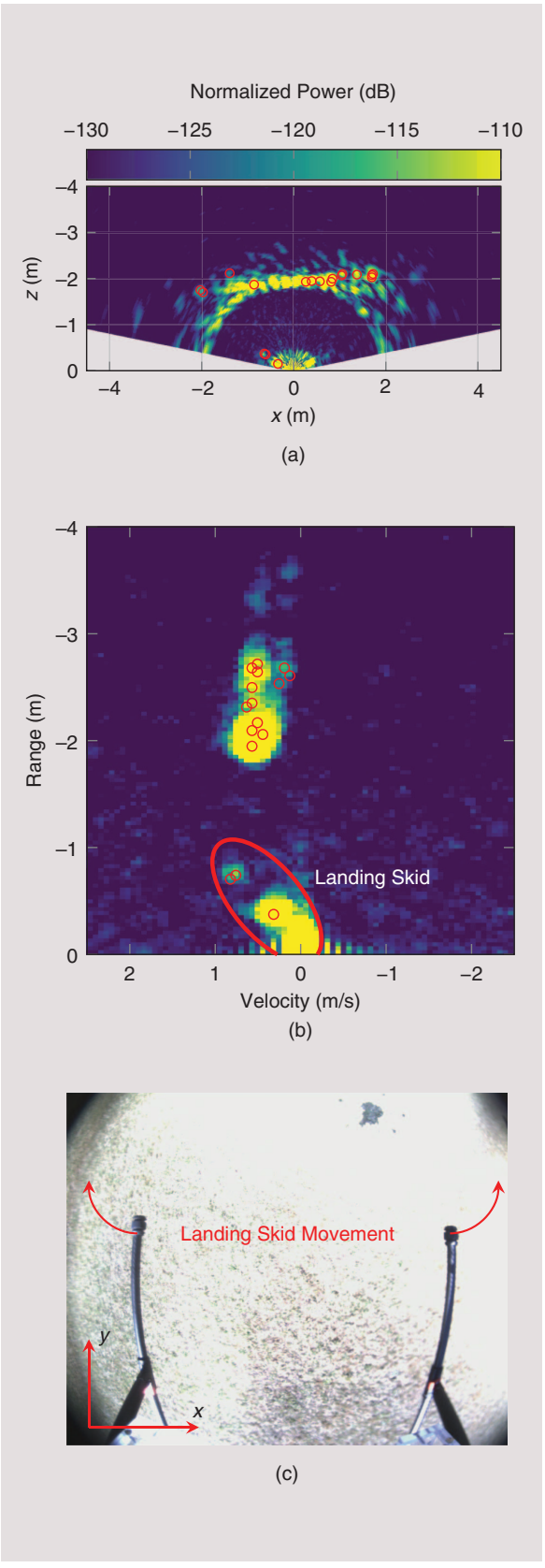

Figure 10. *The measurement of a takeoff with the landing skid being retracted: (a) a ground profile plot in the* xz *plane, (b) a range–velocity diagram, and (c) a bird's-eye view of the scenario. Detected targets are marked with small red circles.*

Experiments with the imaging radar facing forward show the ability to survey a broad area in front of the UAV.

diagram and is marked red in Figure 10(b). The landing skid is very close, so multiple reflections between it and the radar are present. This could be used to check whether the landing skid is ready before touchdown.

A measurement by the UAV flying over 1.2-m-high stepped stone masonry is considered next. The aerial vehicle is moving with a constant velocity in the y direction. The ground profile has two clearly distinguishable levels, and there are nearly no velocity components present. The measured ground profile is depicted in Figure 11(a) and the scenario from a side view in Figure 11(c). Two distinct levels at approximately −4.2 and −5.4 m are present, as expected. In the encircled area, the steep masonry can be seen. Compared to the previous measurement shown in

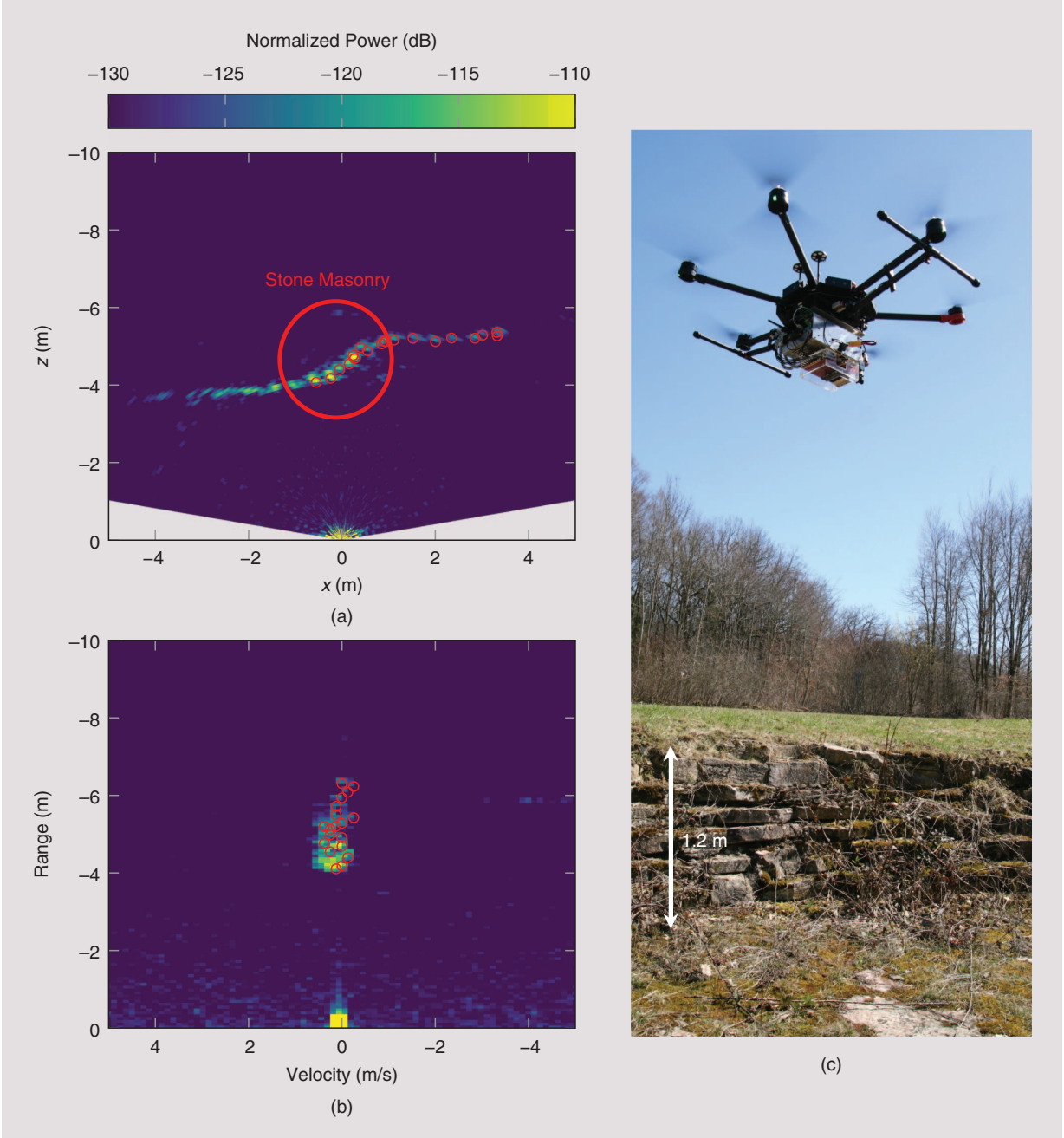

Figure 11. *The measurement of the ground profile of an area of stone masonry: (a) a radar ground profile in the* xz *plane, (b) a range–velocity plot, and (c) a photo of the UAV flying to the side of the stone masonry. Detected targets are marked with small red circles.*

Figure 10(a), it is obvious that the landing skid is retracted and no longer visible as a close target. Considering the range–velocity diagram depicted in Figure 11(b), widely spread targets in the range direction, with almost no velocity components, are visible between −4 and −6 m.

This experiment shows that an imaging radar can provide highly detailed ground profiles with a single measurement. Because UAVs are trending toward greater autonomy, they must also perform autonomous landing maneuvers in case of emergency. A UAV equipped with an imaging radar could determine a suitable landing area based on the measured ground profile.

Forward-Facing Measurements

With the imaging radar in the forward-facing orientation, scenarios for obstacle detection and collision avoidance are considered. In this setup, the antenna beam in azimuth again covers the x axis, and the antenna beam in elevation covers the z axis, as depicted in Figure 8(a) and (b). The orientation of the camera is adjusted to have a first-person view (FPV) of the UAV and the radar.

At first, a measurement with the UAV moving alongside a high metal fence at a speed of approximately 5 m/s is considered (Figure 12). A photo from the FPV perspective is provided in Figure 12(c). Because of the FoV of ±40° in the x direction, it is expected that even closely spaced fenceposts should be visible in the xy plane. The subsequent fenceposts and other parts of the fence between the posts are visible at distances greater than 10 m. Based on the range–velocity diagram in Figure 12(b), we see that the targets are distributed over the velocity in a cosine-shaped manner, which can be derived from the dependency of the Doppler frequency on the cosine of the angle of arrival.

Second, the collision-avoidance capability is investigated with a moving target while the UAV with the mounted imaging radar is hovering at a fixed altitude. A second, smaller UAV (a DJI Phantom 3 with a body diameter of 30 cm, excluding the propellers) is used as a target. The target is flying by from the front right, heading to the rear left. Two snapshots, separated by 740 ms from the FPV perspective, are depicted in Figure 13(a), with the photo on the left side representing the earlier point in time. As can be observed in the xy diagram of Figure 13(b), even this relatively small UAV can be clearly detected and located. It is possible to extract the radial velocity from the range–velocity diagram of Figure 13(c). From snapshot to snapshot, the route of the target can be followed. Several consecutive measurements could be evaluated to estimate the target's orientation and trajectory. With the trajectory and the direct velocity measurement, the flight controller can monitor whether a collision is imminent and perform an evasive maneuver.

The relatively high frequencies enable small and lightweight sensors, making radar feasible for even small unmanned aircraft.

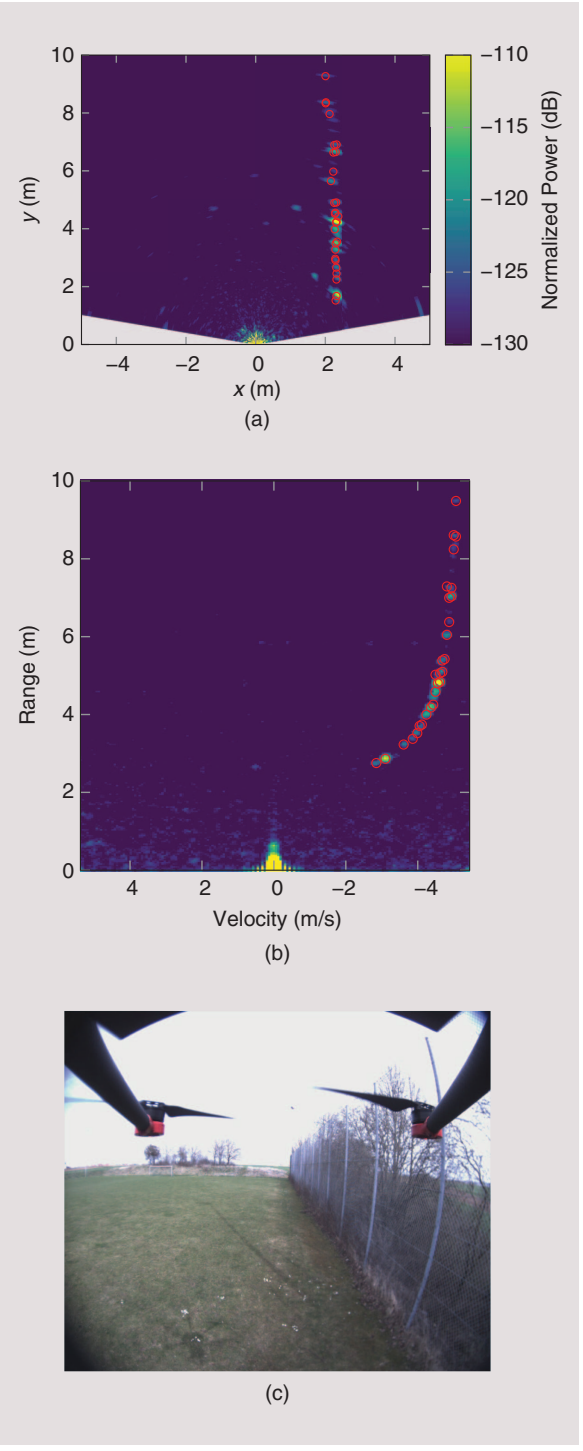

Figure 12. *A UAV with forward-facing imaging radar moving alongside a high metal fence: (a) the measurements for a front view in the* xy *plane, (b) the measurements for range and velocity, and (c) an FPV. Detected targets are marked with small red circles.*

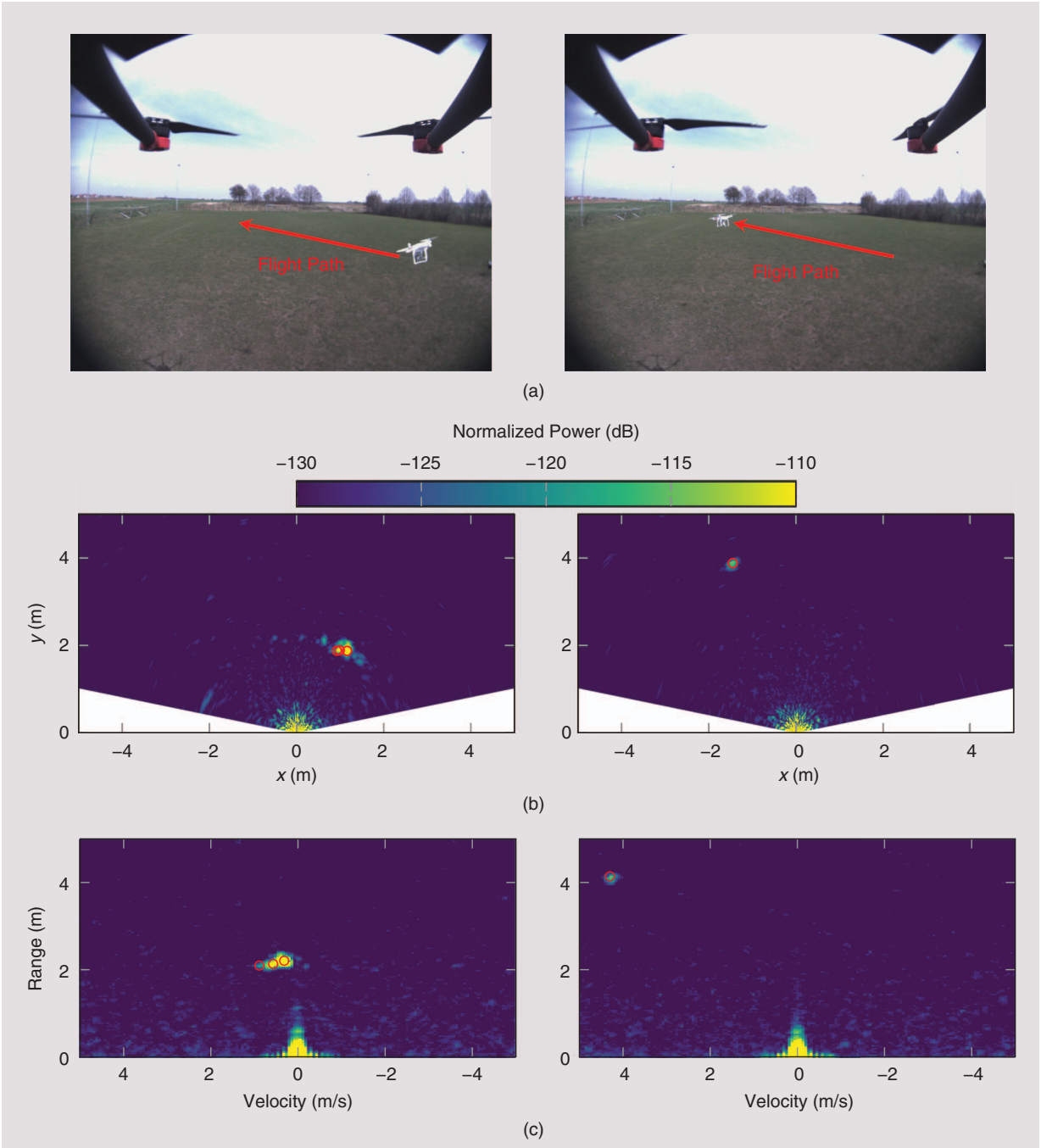

Figure 13. *(a) A camera image from an FPV shows a small drone (a DJI Phantom 3) with a diameter of approximately 30 cm, excluding its propellers, passing by from right to left. Two snapshots separated by 740 ms depict (b) radar measurements in the* xy *plane and (c) a range–velocity diagram. Detected targets are marked with small red circles.*

Conclusions

High flexibility and easy usability boost the popularity of UAVs in consumer and industrial applications, ranging from autonomous parcel delivery to agriculture. Using unmanned aircraft as a sensor platform for SAR and GPR is not the only use for radar. Radar can provide reliable data where other state-of-the-art sensors attached to UAVs reach their limit, e.g., in cases of low contrast or backlight in vision-based systems. It has been shown that measuring the altitude AGL is a simple task with a radar sensor. Additionally, detailed sections of a terrain profile can be obtained with a single radar measurement, using a 3×8-channel TDM MIMO radar with a 2-GHz bandwidth at a center frequency of 76.5 GHz and chirp-sequence frequency modulation.

Further experiments with the imaging radar facing forward show the ability to survey a broad area in front of the UAV, with the capability of simultaneous

multitarget range, velocity, and angle measurement. Targets in an angular range of up to ±60° in azimuth have been detected. Even small UAVs passing by could be observed. With appropriate tracking algorithms and trajectory estimation, collision avoidance and evasive maneuvering could be realized.

With the integration of complete radar front ends on single chips (which are becoming available in the ISM bands at 60 and 122 GHz), bolstered by the results of the survey presented here, radar can increase the sensing capability and safety of UAVs. The relatively high frequencies enable small and lightweight sensors, making radar feasible for even small unmanned aircraft.

Acknowledgment

This work was partly supported by the Ministry for Science, Research, and Arts Baden-Württemberg in the ZAFH MikroSens project.

References

[1] S. Jordan, J. Moore, S. Hovet, J. Box, J. Perry, K. Kirsche, D. Lewis, and Z. T. H. Tse, "State-of-the-art technologies for UAV inspections," *IET Radar, Sonar Navigation*, vol. 12, pp. 151–164, Feb. 2018.

[2] S. Krause, F. Hartmann, and J.-P. Mund, "UAV workflow optimization for the acquisition of high-quality photogrammetric point clouds in forestry," *GI-Forum: J. Geograph. Inform. Sci.*, vol. 1, pp. 72–84, 2016. doi:10.1553/giscience2016_01_s72.

[3] J. Zhang, J. Hu, J. Lian, Z. Fan, X. Ouyang, and W. Ye, "Seeing the forest from drones: Testing the potential of lightweight drones as a tool for long-term forest monitoring," *Biolog. Conserv.*, vol. 198, pp. 60–69, June 2016.

[4] Deutsche Post DHL. (2014, Sept. 24). DHL parcelcopter launches initial operations for research purposes. [Online]. Available: http://www.dhl.com/en/press/releases/releases_2014/group/dhl_parcelcopter_launches_initial_operations_for_research_purposes.html

[5] Deutsche Post DHL. (2016, Feb. 11). Successful trial integration of DHL Parcelcopter into logistics chain. [Online]. Available: https://www.dhl-in-motion.com/dr1/article/successful-trial-integration-of-dhl-parcelcopter-into-logistics-chain

[6] P. Patel, "Agriculture drones are finally cleared for takeoff," *IEEE Spectr.*, vol. 53, no. 11, pp. 13–14, 2016.

[7] *AGRAS MG-1S User Manual V1.0*, DJI, Shenzhen, China, 2017.

[8] M. Schartel, R. Burr, P. Schoeder, G. Rossi, P. Hügler, W. Mayer, and C. Waldschmidt, "Radar-based altitude over ground estimation of UAVs," in *Proc. German Microwave Conf. (GeMiC)*, 2018, pp. 103–106.

[9] M. Schartel, R. Burr, W. Mayer, N. Docci, and C. Waldschmidt, "UAV-based ground penetrating synthetic aperture radar," in *Proc. IEEE MTT-S Int. Conf. Microwaves Intelligent Mobility (ICMIM)*, 2018, pp. 1–4.

[10] *MAVIC AIR User Manual V1.2*, DJI, Shenzhen, China, 2018.

[11] P. Hügler, M. Geiger, and C. Waldschmidt, "77 GHz radar-based altimeter for unmanned aerial vehicles," in *Proc. IEEE Radio and Wireless Symposium (RWS)*, 2018, pp. 129–132.

[12] *AGRAS MG-1S Obstacle Avoidance Radar V1.0*, DJI, Shenzhen, China, 2017.

[13] H. Essen, W. Johannes, S. Stanko, R. Sommer, A. Wahlen, and J. Wilcke, "High resolution W-band UAV SAR," in *Proc. IEEE Int. Geoscience and Remote Sensing Symp.*, 2012, pp. 5033–5036.

[14] C. J. Li and H. Ling, "Synthetic aperture radar imaging using a small consumer drone," in *Proc. IEEE Int. Symp. Antennas and Propagation USNC/URSI National Radio Science Meeting*, 2015, pp. 685–686.

[15] G. Fasano, A. Renga, A. R. Vetrella, G. Ludeno, I. Catapano, and F. Soldovieri, "Proof of concept of micro-UAV-based radar imaging," in *Proc. Int. Conf. Unmanned Aircraft Systems (ICUAS)*, 2017, pp. 1316–1323.

[16] G. Ludeno, I. Catapano, G. Gennarelli, F. Soldovieri, A. R. Vetrella, A. Renga, and G. Fasano, "A micro-UAV-borne system for radar imaging: A feasibility study," in *Proc. 9th Int. Workshop Advanced Ground Penetrating Radar (IWAGPR)*, 2017, pp. 1–4.

[17] M. Schuetz, M. Oesterlein, C. Birkenhauer, and M. Vossiek, "A custom lightweight UAV for radar remote sensing: Concept design, properties and possible applications," in *Proc. IEEE MTT-S Int. Conf. Microwaves Intelligent Mobility (ICMIM)*, 2017, pp. 107–110.

[18] A. Moses, M. J. Rutherford, M. Kontitsis, and K. P. Valavanis, "UAV-borne X-band radar for collision avoidance," *Robotica*, vol. 32, no. 1, pp. 97–114, 2014.

[19] A. F. Scannapieco, A. Renga, G. Fasano, and A. Moccia, "Ultralight radar sensor for autonomous operations by micro-UAS," in *Proc. Int. Conf. Unmanned Aircraft Systems (ICUAS)*, 2016, pp. 727–735.

[20] W. Liu, C. Yu, X. Wang, Y. Zhang, and Y. Yu, "The altitude hold algorithm of UAV based on millimeter wave radar sensors," in *Proc. 9th Int. Conf. Intelligent Human-Machine Systems and Cybernetics (IHMSC)*, vol. 1, 2017, pp. 436–439.

[21] J. Hasch, E. Topak, R. Schnabel, T. Zwick, R. Weigel, and C. Waldschmidt, "Millimeter-wave technology for automotive radar sensors in the 77 GHz frequency band," *IEEE Trans. Microw. Theory Techn.*, vol. 60, no. 3, pp. 845–860, 2012.

[22] C. Waldschmidt and H. Meinel, "Future trends and directions in radar concerning the application for autonomous driving," in *Proc. 44th European Microwave Conf.*, 2014, pp. 1719–1722.

[23] C. Beck, H. J. Ng, R. Agethen, M. PourMousavi, H. P. Forstner, M. Wojnowski, K. Pressel, R. Weigel, A. Hagelauer, and D. Kissinger, "Industrial mmWave radar sensor in embedded wafer-level BGA packaging technology," *IEEE Sensors J.*, vol. 16, no. 17, pp. 6566–6578, 2016.

[24] A. Hagelauer, M. Wojnowski, K. Pressel, R. Weigel, and D. Kissinger, "Integrated systems-in-package: Heterogeneous integration of millimeter-wave active circuits and passives in fan-out wafer-level packaging technologies," *IEEE Microw. Mag.*, vol. 19, no. 1, pp. 48–56, 2018.

[25] M. Hitzler, L. Boehm, W. Mayer, and C. Waldschmidt, "Radiation pattern optimization for QFN packages with on-chip antennas at 160 GHz," *IEEE Trans. Antennas Propag.*, pp. 1–1, 2018.

[26] V. Winkler, "Range Doppler detection for automotive FMCW Radars," in *Proc. European Radar Conf. (EuRAD)*, 2007, pp. 166–169.

[27] C. Schroeder and H. Rohling, "X-band FMCW radar system with variable chirp duration," in *Proc. IEEE Radar Conf.*, 2010, pp. 1255–1259.

[28] J. J. M. de Wit, W. L. van Rossum, and A. J. de Jong, "Orthogonal waveforms for FMCW MIMO radar," in *Proc. IEEE RadarCon (RADAR)*, 2011, pp. 686–691.

[29] R. Schmidt, "Multiple emitter location and signal parameter estimation," *IEEE Trans. Antennas Propag.*, vol. 34, no. 3, pp. 276–280, 1986.

[30] P. Stoica and K. C. Sharman, "Maximum likelihood methods for direction-of-arrival estimation," *IEEE Trans. Acoustics, Speech, Signal Process.*, vol. 38, no. 7, pp. 1132–1143, 1990.

[31] P. Häcker and B. Yang, "Single snapshot DOA estimation," *Advances Radio Sci.*, vol. 8, pp. 251–256, 2010. doi: 10.5194/ars-8-251-2010.

[32] E. Topak, J. Hasch, and T. Zwick, "Compact topside millimeter-wave waveguide-to-microstrip transitions," *IEEE Microw. Compon. Lett.*, vol. 23, no. 12, pp. 641–643, 2013.

[33] C. Vasanelli, R. Batra, A. D. Serio, F. Boegelsack, and C. Waldschmidt, "Assessment of a millimeter-wave antenna system for MIMO radar applications," *IEEE Antennas Wireless Propag. Lett.*, vol. 16, pp. 1261–1264, Nov. 2017.

[34] C. Schmid, R. Feger, C. Pfeffer, and A. Stelzer, "Motion compensation and efficient array design for TDMA FMCW MIMO radar systems," in *Proc. 6th European Conf. Antennas and Propagation (EUCAP)*, 2012, pp. 1746–1750.

[35] J. Bechter, F. Roos, and C. Waldschmidt, "Compensation of motion-induced phase errors in TDM MIMO radars," *IEEE Microw. Compon. Lett.*, vol. 27, no. 12, pp. 1164–1166, 2017.

[36] F. Roos, J. Bechter, N. Appenrodt, J. Dickmann, and C. Waldschmidt, "Enhancement of Doppler unambiguity for chirp-sequence modulated TDM-MIMO radars," in *Proc. Int. Conf. Microwaves Intelligent Mobility (ICMIM)*, 2018, pp. 1–4.